Superadiabatic evolution of acoustic and vorticity perturbations in Couette flow

Gael Favraud* and Vincent Pagneux
LUNAM Université, LAUM (Laboratoire d'Acoustique de l'Université du Maine), UMR CNRS 6613, Avenue Olivier Messiaen, 72085 Le Mans Cedex 9, France
(Received 21 May 2013; revised manuscript received 7 January 2014; published 14 March 2014)

Nonadiabatic transitions between the acoustic and the vorticity modes perturbing a plane Couette flow are examined in the context of higher-order WKB asymptotics. In the case of the Schrödinger equation, it is known that looking at the solution expressed in the superadiabatic base, composed of higher-order asymptotic solutions, smoothes quantum state transitions. Then, increasing the order of the superadiabatic base causes these transitions to tend to the Gauss error function, and, once an optimal order is reached, the asymptotic process starts to diverge. We show that for perturbations in Couette flow, similar results can be applied on the amplitudes of the vorticity and acoustic modes. This allows us to more closely track the emergence of the acoustic modes in the presence of the vorticity mode.

DOI: 10.1103/PhysRevE.89.033012 PACS number(s): 47.35.Rs, 43.28.+h, 43.20.+g, 47.20.−k

I. INTRODUCTION

The propagation of acoustic waves in a Couette plane flow (and *a fortiori* in shear flows) allows the existence of subtle phenomena of couplings between acoustic and vorticity perturbations (for a review, see [1]). For the stability analysis of this flow, the classical stability analysis based on the study of the eigenvalues of the linearized equations governing perturbations is known to give erroneous results, due to the presence of transient growths [2–4]. Inspired by the earlier works of Kelvin [5], a new approach, the so called *nonmodal approach*, was developed and used to study the coupling phenomena between vorticity and acoustic perturbations in a Couette plane flow [1,6–15]. In this particular case, this approach allows a great number of simplifications. Indeed, the linearity of the flow allows us to reduce the Euler equations governing the time evolution of compressible perturbations into a first-order ordinary differential equation in time of dimension 3. This process relies on two steps. The first step is to introduce a convected coordinate frame following the flow, which turns the linearized Euler equations into equations with space-independent coefficients. Then, taking advantage of having space-independent coefficients, the second step is to apply a space Fourier transform, which gives the above-mentioned ordinary differential equation governing the time evolution of each spatial Fourier harmonic.

In previous works, this system was treated by deriving a second-order inhomogeneous equation on the horizontal component of the velocity field of the perturbation [7]. It was first reported, in the case of incompressible perturbations, that the wave vector of any spatial Fourier harmonic is subject to a time evolution due to the effect of the flow [6]. The vertical components of the wave vector decrease linearly over time, so that at a particular time $\tau_\star$ the wave vector is horizontal. A direct consequence of this phenomenon is that the wave-vector amplitude reaches a minimum for that $\tau_\star$ time. An important parameter involved in the physics of this flow is the ratio of the shear rate of the flow over the characteristic frequency of the perturbations, which we call here ε (it is called R in Refs. [1,6–15]). In the case of compressible perturbations, the governing equations permit the existence of two types of perturbations: two acoustic modes of perturbation were identified as the solutions of the associated homogeneous equation, while a vorticity mode of perturbation was identified as the particular solution of the whole inhomogeneous equation. This vorticity mode, which corresponds to the transient growth of the incompressible case, can reach arbitrarily high amplitudes in finite time. The acoustic modes also display a particular behavior. A mechanism of energy exchange between acoustic perturbations and the mean flow has been exhibited [7–9]. The acoustic waves are able to give or extract energy from the mean flow depending on whether the time is smaller or larger than $\tau_\star$. It has also been recovered that acoustic waves in such a flow acquire a vortical behavior [16], which gets more important as ε is larger. But the most interesting phenomenon, which is the main subject of this paper, is the coupling between these modes, allowing the generation of acoustic waves from vorticity waves [10].

In another paper [17] we show that using the Wentzel-Kramer-Brillouin (WKB) method gives an efficient frame to describe the different types of perturbations in a general linear planar flow. With this method, we addressed the known problem of the generation of acoustic waves by the vorticity wave, but also another coupling phenomenon, namely the generation of an acoustic wave by the acoustic wave propagating in the opposite direction. The method we proposed relies on the existence of a small parameter ε, which is the ratio of the shear rate of the mean flow to the frequency of the perturbation, to provide approximate asymptotic solutions. At order ε, the solutions given by the WKB method are able to describe very closely the exact solution. The only phenomena which are not taken into account are sudden emergences of nonexcited modes which occur near the complex degeneracies of the equation governing the time evolution of the perturbations. These emergences are exponentially small quantities of order $e^{-C/\varepsilon}$, for some constant C, which cannot be taken into account by asymptotic methods (due to the fact that all derivatives of $e^{-C/\varepsilon}$ with respect to ε are null at zero [18]). Similar phenomena, called nonadiabatic transitions, have been studied in quantum

*gael.favraud@univ-lemans.fr

mechanics since the works of Landau [19,20] and Zener [21]. The use of higher-order approximations provides a base of asymptotic approximate solutions, or modes, which is called the *superadiabatic* base [22]. Contrary to the adiabatic base that is composed of approximations in which only the first term (or a given number of terms) is retained, the superadiabatic base is composed of approximations truncated at an optimal order which depends on ε. Looking at the exact solution expressed in this superadiabatic base allows for a finer tracking of the emerging mode amplitudes by smoothing them [22]. At the optimal order, the time evolution of the amplitude of the emerging mode renormalizes to a general shape, which is the Gauss error function. Then, as in many asymptotic processes [18], it starts to diverge once this optimal order is reached. This has been predicted in the case of a two-state system by Berry and Lim [22,23] on the basis of the work done by Dykhne [24] and by Davis and Pechukas [25]. More recently, a mathematical proof was proposed by Hagedorn and Joye [26]. Similar renormalizations of amplitudes are depicted, among others, in Ref. [27] for a two-level system, in Ref. [28] concerning the case of two successive coupling areas, and in Ref. [29] concerning a three-level system.

In this paper, we address the coupling phenomenon between acoustic and vorticity linear perturbations of a planar Couette flow, where superadiabatic bases can be used. In the first section, the equations governing the evolution of the perturbations are derived following the nonmodal approach, as in Ref. [7]. In Sec. II, the WKB method is applied in such a context. The first-order asymptotic solution gives us a base of three modes: two acoustic modes and one vorticity mode. We show that this base is composed of three modes close to exact solutions and enables us to track the emergences of nonexcited modes. In the final section, we derive the superadiabatic bases corresponding to the following orders. The predictions of Berry are investigated in our case.

II. MODEL

Let us consider a mean plane Couette flow,

$$\mathbf{u}_0(x,y) = Ay\hat{\mathbf{e}}_x, \tag{1a}$$

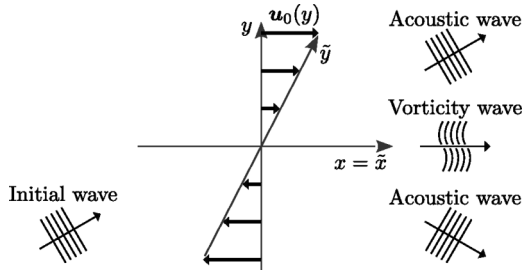

FIG. 1. Sketch of the studied problem. The bold arrows represent the mean flow velocity field $\mathbf{u}_0(y) = Ay\hat{\mathbf{e}}_x$. The convected coordinates $(\tilde{x},\tilde{y})$ introduced by the change of variables in Eq. (3) "follow" the flow.

where A is the shear rate of the flow, as represented in Fig. 1. The most interesting thing about this choice is that in this case the nonmodal method consists in considering the evolution of dimensionless spatial Fourier harmonics in the convected coordinate frame which follows the flow. This can be reduced to two major steps. The first step is to introduce a set of independent variables which will be a frame of convected coordinates, and the second step is to apply the spatial Fourier transform to the equations. This derivation of the equations has now become quite classical and is commonly used [1,6–15,17], and it can be generalized to more general linear two-dimensional (2D) flows [12,17].

We introduce compressible perturbations of pressure p and velocity $\mathbf{u} = (u,v)$. For small amplitudes, the time evolution of these perturbations is governed by the linearized Euler equations

$$\left(\frac{\partial}{\partial t} + Ay\frac{\partial}{\partial x}\right)u + Av = -\frac{1}{\rho_0}\frac{\partial}{\partial x}p, \tag{2a}$$

$$\left(\frac{\partial}{\partial t} + Ay\frac{\partial}{\partial x}\right)v = -\frac{1}{\rho_0}\frac{\partial}{\partial y}p, \tag{2b}$$

$$\left(\frac{\partial}{\partial t} + Ay\frac{\partial}{\partial x}\right)p = -\rho_0 c_0^2\left(\frac{\partial}{\partial x}u + \frac{\partial}{\partial y}v\right), \tag{2c}$$

where c_0 is the adiabatic speed of sound linking the density and pressure of the perturbations by $p = c_0^2\rho$, and where ρ_0 is the mean density in the mean flow. Equations (2) govern the evolution of acoustic and vorticity perturbations in the mean flow $\mathbf{u}_0$.

As a first step, we define the convected coordinate frame

$$\tilde{x} = x - Ayt, \tag{3a}$$

$$\tilde{y} = y, \tag{3b}$$

$$\tilde{t} = t, \tag{3c}$$

and rewrite Eqs. (2) in terms of these variables,

$$\frac{\partial}{\partial\tilde{t}}u + Av = -\frac{1}{\rho_0}\frac{\partial}{\partial\tilde{x}}p, \tag{4a}$$

$$\frac{\partial}{\partial\tilde{t}}v = -\frac{1}{\rho_0}\left(\frac{\partial}{\partial\tilde{y}} - A\tilde{t}\frac{\partial}{\partial\tilde{x}}\right)p, \tag{4b}$$

$$\frac{\partial}{\partial\tilde{t}}p = -\rho_0 c_0^2\left[\frac{\partial}{\partial\tilde{x}}u + \left(\frac{\partial}{\partial\tilde{y}} - A\tilde{t}\frac{\partial}{\partial\tilde{x}}\right)v\right]. \tag{4c}$$

Since these equations have space-independent coefficients, we are going to apply a Fourier transform. This is equivalent to looking for solutions in the form of plane waves in the convected coordinates:

$$\begin{bmatrix} u(\tilde{x},\tilde{y},\tilde{t}) \\ v(\tilde{x},\tilde{y},\tilde{t}) \\ p(\tilde{x},\tilde{y},\tilde{t}) \end{bmatrix} = \begin{bmatrix} \tilde{u}(\tilde{t}) \\ \tilde{v}(\tilde{t}) \\ \tilde{p}(\tilde{t}) \end{bmatrix} e^{i\alpha_0\tilde{x}+i\beta_0\tilde{y}}, \tag{5}$$

where α_0 and β_0 are the horizontal and vertical Fourier wave numbers in the convected coordinates $(\tilde{x},\tilde{y},\tilde{t})$. As a consequence, Eqs. (4) become the following system of three

ordinary differential equations in time:

$$\frac{\partial}{\partial \tilde{t}}\tilde{u} + A\tilde{v} = -\frac{1}{\rho_0} i\alpha_0 \tilde{p}, \tag{6a}$$

$$\frac{\partial}{\partial \tilde{t}}\tilde{v} = -\frac{1}{\rho_0} i(\beta_0 - \alpha_0 A\tilde{t})\tilde{p}, \tag{6b}$$

$$\frac{\partial}{\partial \tilde{t}}\tilde{p} = -\rho_0 c_0^2 [i\alpha_0 \tilde{u} + i(\beta_0 - \alpha_0 A\tilde{t})\tilde{v}]. \tag{6c}$$

To obtain dimensionless forms of Eqs. (6), we use $1/\alpha_0$ as a reference value for distances, and commonly used reference values for the other quantities. So we introduce the dimensionless variables $X = \alpha_0 \tilde{x}$, $Y = \alpha_0 \tilde{y}$, $T = c_0 \alpha_0 \tilde{t}$, $U(X,Y,T) = \frac{1}{c_0}\tilde{u}(\tilde{x},\tilde{y},\tilde{t})$, $V(X,Y,T) = \frac{1}{c_0}\tilde{v}(\tilde{x},\tilde{y},\tilde{t})$, and $P(X,Y,T) = \frac{1}{\rho_0 c_0^2}\tilde{p}(\tilde{x},\tilde{y},\tilde{t})$. Eventually, rewriting Eqs. (6) in terms of these dimensionless variables leads to

$$\dot{U}(T) + \varepsilon V(T) = -i P(T), \tag{7a}$$

$$\dot{V}(T) = -i\beta(\varepsilon T)P(T), \tag{7b}$$

$$\dot{P}(T) = -iU(T) - i\beta(\varepsilon T)V(T), \tag{7c}$$

where the dimensionless parameter appears,

$$\varepsilon = \frac{A}{c_0 \alpha_0}, \tag{8}$$

and where $\beta(\varepsilon T) = \beta_0/\alpha_0 - \varepsilon T$. This ε, considered as the small parameter, is the ratio of the shear rate of the mean flow to the frequency of the perturbation. The system of Eqs. (7) forms an ordinary differential equation of dimension 3 with respect to the dimensionless time.

When $\varepsilon = 0$, the classical wave equation can be recovered from Eqs. (7) [as well as from Eqs. (2)]. Hereafter, in order to construct asymptotic solutions with use of the WKB method, we focus on small values of ε, namely $\varepsilon \ll 1$. This corresponds to a small shearing assumption, that is, a weak shear rate of the mean flow compared to the frequency of the perturbations. In that case, the characteristic time scale of the variation of β is εT (slow variation), whereas it is known from classical acoustics that the solution oscillates on the T time scale. Hence we introduce the slow time defined by

$$\tau = \varepsilon T, \tag{9}$$

and rewrite Eqs. (7) in terms of τ. This yields

$$\varepsilon \dot{\mathbf{X}}(\tau) = [H_0(\tau) + \varepsilon H_1]\mathbf{X}(\tau), \tag{10}$$

where $\mathbf{X}(\tau) = (U(\tau), V(\tau), iP(\tau))$, and

$$H_0(\tau) = \begin{bmatrix} 0 & 0 & -1 \\ 0 & 0 & -\beta(\tau) \\ 1 & \beta(\tau) & 0 \end{bmatrix}, \quad H_1 = \begin{bmatrix} 0 & -1 & 0 \\ 0 & 0 & 0 \\ 0 & 0 & 0 \end{bmatrix}. \tag{11}$$

Here and hereafter, the overdot denotes the derivative with respect to the slow time τ.

Note that multiplying Eq. (10) by the imaginary unit i yields a Schrödinger-like equation whose Hamiltonian $(iH_0 + i\varepsilon H_1)$ is *not* Hermitian due to the $i\varepsilon H_1$ part. That system has to be compared with one of the examples studied by Berry,

$$i\varepsilon \dot{\mathbf{X}} = H_0(\tau)\mathbf{X} \tag{12}$$

with

$$H_0(\tau) = \begin{bmatrix} \tau & 1 \\ 1 & -\tau \end{bmatrix}. \tag{13}$$

As can be seen from Eqs. (10) and (11), the β function plays a very important role since, being given an initial condition at a time τ_i, it fully determines the whole dynamic of the perturbations. To give a better understanding of what β corresponds to, let us first write β in terms of the slow time τ:

$$\beta(\tau) = \frac{\beta_0}{\alpha_0} - \tau. \tag{14}$$

Then, we point out that the spatial exponential dependence of the solution in the convected coordinates $(\tilde{x},\tilde{y})$, described in Eq. (5), can be rewritten in the original coordinates (x,y)

$$e^{i\alpha_0 \tilde{x} + i\beta_0 \tilde{y}} = e^{i\alpha_0 [x + \beta(\tau) y]}. \tag{15}$$

This means that, while $\mathbf{k}_0 = (\alpha_0, \beta_0)$ is the wave vector with respect to the convected coordinates $\tilde{x}$ and $\tilde{y}$, $\mathbf{k}(\tau) = (1, \beta(\tau))$ acts as an instantaneous wave vector with respect to the original coordinates x and y (up to the nondimensionalization factor α_0). In fact, it can be seen in Eq. (11) that the H_0 matrix is composed of the two components of $\mathbf{k}$, one of which is constant in the present case of a Couette flow (in the case of more general linear flows, the two components may vary in time [12,17]). This wave vector $\mathbf{k}$ evolves in time and is shifted along the y axis because of the time evolution of its vertical component, β. At the particular time $\tau_\star = \beta_0/\alpha_0$, β is zero, $\mathbf{k}$ is horizontal, and the norm of $\mathbf{k}$ reaches a minimum. As explained in the following sections, this time $\tau_\star$ will play a very important role since couplings phenomena occur at this time.

Equation (14) shows that β only depends on β_0/α_0 and ε. The β_0/α_0 parameter defines the vertical component of the wave vector at the time $\tau = 0$, but also, as just mentioned, the time at which the coupling phenomena occur. Considering a particular value of β_0/α_0 is equivalent to shifting the τ time axis. For instance, introducing a change of variable $\tilde{\tau} = \tau - \beta_0/\alpha_0$ shows that any case can reduce to the case in which $\beta_0 = 0$, provided that the initial condition is also shifted in time accordingly. Put another way, we can say that choosing a different β_0 only advances or postpones the coupling time $\tau_\star$. Therefore, without loss of generality, we can choose arbitrary β_0. Here and hereafter we take $\beta_0 = 0$ for convenience, so that $\tau_\star = 0$. A sketch of the evolution of the wave vector is given in Fig. 2 for that case. Other illustrations of this phenomenon can be found in Ref. [17] for other linear flows.

III. THE ADIABATIC BASE

The WKB method (see, for instance, [30]), sometimes called the WKBJ method (J stands for Jeffrey) or the "Liouville-Green" method, belongs to multiple scale asymptotic methods, and it relies on the use of a small parameter, here ε. It consists in looking for a solution under the form of the ansatz

$$\mathbf{X}^{(n)}(\tau) = e^{\frac{i}{\varepsilon}\sigma(\tau)}[\boldsymbol{\varphi}^{(0)}(\tau) + \cdots + \varepsilon^n \boldsymbol{\varphi}^{(n)}(\tau)], \tag{16}$$

where the scalar phase $\sigma(\tau)$ and the vectorial series terms $\boldsymbol{\varphi}^{(n)}(\tau)$ are the unknowns to be determined. The main idea

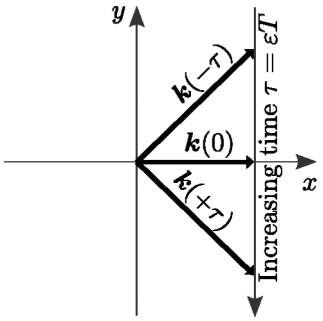

FIG. 2. Sketch of the time evolution of the dimensionless wave vector $\mathbf{k} = (1, \beta(\tau))$.

behind this method is to describe two phenomena. One phenomenon is the rapidly oscillating behavior of the solution which occurs on the fast time scale T and is described by the exponential factor. The second phenomenon is the slow variation of the way the solution oscillates which occurs on the slow time scale τ and is described by the series.

Inserting (16) into (10) yields the successive equations for each order of power of ε,

$$(i\dot{\sigma} - H_0) \quad \boldsymbol{\varphi}^{(0)} = \mathbf{0}, \tag{17}$$

$$(i\dot{\sigma} - H_0) \quad \boldsymbol{\varphi}^{(n+1)} = H_0\boldsymbol{\varphi}^{(n)} - \varepsilon H_1 \dot{\boldsymbol{\varphi}}^{(n)}. \tag{18}$$

According to the order 0 equation [Eq. (17)], $i\dot{\sigma}$ is an eigenvalue of the H_0 matrix and $\boldsymbol{\varphi}^{(0)}$ is its associated eigenvector. These eigenvalues are

$$\lambda_H = 0, \quad \lambda_\pm = \pm ik, \tag{19}$$

where $k = \sqrt{1+\beta^2}$ is the norm of $\mathbf{k}$. The evolution of the eigenvalues (purely imaginary) is represented in Fig. 3. As mentioned in the preceding section, at $\tau = 0$, k reaches a minimum, and the three eigenvalues are the closest to each other. As detailed later, this particular time is of crucial interest as couplings occur at this time.

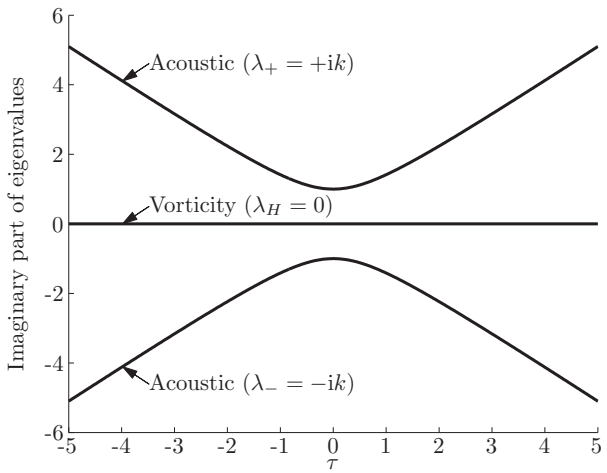

FIG. 3. Time evolution of the imaginary parts of the eigenvalues of the H_0 matrix (real parts are zeros) for $\varepsilon = 0.2$.

The associated modes are

$$\boldsymbol{\varphi}_H^{(0)} = \frac{1}{k^2}\begin{bmatrix}\beta\\-1\\0\end{bmatrix}, \quad \boldsymbol{\varphi}_\pm^{(0)} = \frac{1}{\sqrt{k}}\begin{bmatrix}1\\\beta\\\mp ik\end{bmatrix}, \tag{20}$$

where the scalar prefactors come from the compatibility condition imposed by Eq. (18) at order $n = 1$. Finally, the three order 0 WKB approximate solutions, which we call order 0 WKB modes, are

$$\mathbf{X}_\pm^{(0)}(\tau) = e^{\int^\tau \pm\frac{i}{\varepsilon}k(s)ds}\,\boldsymbol{\varphi}_\pm^{(0)}(\tau), \tag{21a}$$

$$\mathbf{X}_H^{(0)}(\tau) = \boldsymbol{\varphi}_H^{(0)}(\tau). \tag{21b}$$

Some subtle phenomena can be understood from the form of these modes and from the time evolution of their amplitudes [17]. By looking at the vectorial form of the $\mathbf{X}_H^{(0)}$ approximate solution, we notice that the velocity components are normal to the wave vector $\mathbf{k}$, and that the pressure perturbation remains null. This means that the complete approximate solution, expressed in terms of u, v, and p, is divergence-free and incompressible, and so we identify $\mathbf{X}_H^{(0)}$ as a vorticity mode of perturbation. On the contrary, the $\mathbf{X}_\pm^{(0)}$ approximate solution has velocity components collinear to $\mathbf{k}$ and an oscillating pressure. Therefore, the associated complete solutions are curl-free and compressible, and we identify them as acoustic modes of perturbation. The fact that the associated velocity field is curl-free is in contradiction with known results [9,16], and the consequences are detailed later. These three modes form a base $\{\mathbf{X}_-^{(0)}; \mathbf{X}_H^{(0)}; \mathbf{X}_+^{(0)}\}$ called the *adiabatic base*. Looking at the exact solution (obtained numerically as explained below) of Eq. (10) in this adiabatic base gives us the amplitude on each WKB mode. By writing $\mathbf{Y}^{(0)}(\tau) = (Y_-^{(0)}(\tau), Y_H^{(0)}(\tau), Y_+^{(0)}(\tau))$, the exact solution $\mathbf{X}(\tau)$ in this adiabatic base, and by defining the transformation matrix $\Phi^{(0)}(\tau) = [\mathbf{X}_-^{(0)}\ \mathbf{X}_H^{(0)}\ \mathbf{X}_+^{(0)}]$, we get

$$\mathbf{X}(\tau) = \Phi^{(0)}(\tau)\mathbf{Y}^{(0)}(\tau), \tag{22}$$

or equivalently $\mathbf{X} = Y_-^{(0)}\mathbf{X}_-^{(0)} + Y_H^{(0)}\mathbf{X}_H^{(0)} + Y_+^{(0)}\mathbf{X}_+^{(0)}$. The WKB approximation predicts that the amplitudes $Y_-^{(0)}$, $Y_H^{(0)}$, and $Y_+^{(0)}$ on each mode of the adiabatic base are constants. On the other hand, for the exact solution of Eq. (10), these components are not constant.

In the following, we focus our study on the time evolution of these mode amplitudes $|Y_H^{(0)}|$, $|Y_+^{(0)}|$ and $|Y_-^{(0)}|$. We first consider the case of an incident acoustic mode, that is, with an initial condition imposed on one of the acoustic modes, $\mathbf{X}(\tau_i) = \mathbf{X}_+^{(0)}(\tau_i)$. Figure 4(a) shows the time evolution of the modulus of each mode amplitude for such an initial condition imposed at $\tau_i = -5$ and for $\varepsilon = 0.2$. The choice of this value of $\varepsilon = 0.2$ is to provide a typical case in which the phenomena can be observed. In experiments, lower values are to be expected, e.g., in a mixing layer where the shear rate would be $A \sim U/L$, with U the velocity difference between the two flows and L the characteristic width of the layer. Supposing that the layer is sufficiently large to contain several wavelengths, say $k_0 L \sim 10$, we would have $\varepsilon = A/(\alpha_0 c_0) \sim U/c_0/10$.

The presented results are obtained by integrating numerically Eq. (10) with a Magnus-Möbius scheme [31–34]. Once the exact solution $\mathbf{X}(\tau)$ is obtained, the mode amplitudes are computed by inverting Eq. (22). Note that we are not

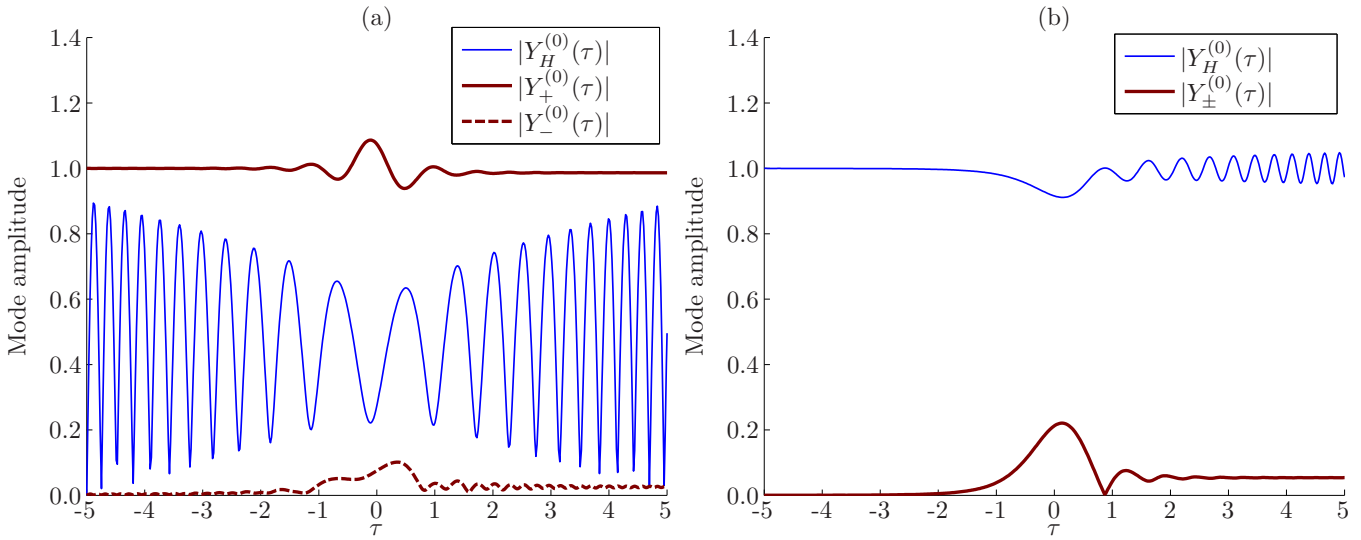

FIG. 4. (Color online) Time evolution of the modulus of the mode amplitudes in the WKB adiabatic base for $\tau_i = -5$ and $\varepsilon = 0.2$, with initial condition (a) on the acoustic "+" mode, $\mathbf{X}(\tau_i) = \mathbf{X}_+^{(0)}(\tau_i)$, and (b) on the vorticity mode, $\mathbf{X}(\tau_i) = \mathbf{X}_H^{(0)}(\tau_i)$. The mode amplitudes $|Y_H^{(0)}(\tau)|$, $|Y_+^{(0)}(\tau)|$, and $|Y_-^{(0)}(\tau)|$ are the projections of the reference numerical solution $\mathbf{X}(\tau)$ on the adiabatic base composed of the vorticity mode $\mathbf{X}_H^{(0)}(\tau)$ and of the two acoustic modes $\mathbf{X}_+^{(0)}(\tau)$ and $\mathbf{X}_-^{(0)}(\tau)$ obtained with the WKB method at order $n = 0$. The mode amplitudes are obtained with the relation $\mathbf{X} = Y_H^{(0)}\mathbf{X}_H^{(0)} + Y_+^{(0)}\mathbf{X}_+^{(0)} + Y_-^{(0)}\mathbf{X}_-^{(0)}$.

looking here at the approximate solutions that constitute the WKB modes, but at the projection of the exact solution of Eq. (10) on the base composed of these WKB modes. This sort of representation is different from the one used in previous works [1,6–15]. This is intended to provide a different physical approach of the involved phenomena by displaying the presence of each mode of perturbation. Our goal is to build the most appropriate base to represent the solution. In the hypothetical case, the WKB modes were exact solutions. These mode amplitudes would be constant over time. A first look at Fig. 4(a) shows that this is not the case here. It shows that for negative times, the incident acoustic "+" mode has an amplitude which stays close to 1, while the amplitude of the acoustic "−" mode remains zero. This means that the adiabatic base managed to cling to an exact solution, since this solution is mostly described by the acoustic "+" mode. However, the vorticity mode immediately appears after the initial time and its amplitude oscillates around a mean value, showing that the current adiabatic base fails to describe an important phenomenon. This is in fact an asymptotic error of order ε, also tackled in Ref. [17]. More physically, this is linked to the fact that the acoustic modes obtained with the WKB method at order $n = 0$ are curl-free, while acoustic waves in shear flows are thought not to be [9,16]. The oscillations of the vorticity mode amplitude correspond to the vorticity part of the exact solution, which is not taken into account in the adiabatic base, leading to an error of order $\varepsilon\sqrt{\tau_i}$ [17]. Near $\tau = 0$, the nonincident acoustic "−" mode, which was null before, emerges. This emergence is very small and is masked by strong oscillations which finally disappear. Then the amplitude stabilizes to a final value, which is very small compared to that of the incident acoustic "+" mode. This emergence is a nonadiabatic transition that the asymptotic process cannot predict as it is an exponentially small phenomenon—of order $e^{-C/\varepsilon}$ for some constant C. This result is very similar to the ones obtained by Berry [23].

Figure 4(b) shows the case of an incident vorticity mode, for the same values of τ_i and ε, and using the same representation as in Fig. 4(a). This case displays behavior comparable to the preceding case in Fig. 4(a): the exact solution is almost completely described by the incident vorticity mode (its amplitude remains 1 and the two others 0), even more precisely than in the preceding case, where a consistent error was present. Then, near $\tau = 0$, a nonadiabatic transition occur, provoking the emergence of two acoustic modes in a similar manner as one acoustic mode provoked the emergence of the other acoustic mode in Fig. 4(a). This transition is more efficient than in the preceding case, and the two acoustic modes have equal amplitudes, indistinguishable in Fig. 4(b). After the transition, the vorticity mode amplitude starts to oscillate, which is the same effect as in Fig. 4(a), here due to the presence of the acoustic mode that has emerged at $\tau = 0$.

Figure 5 shows the time evolution of the mode amplitudes but for $\varepsilon = 0.1$. The same phenomenon can be seen in Fig. 5(a) with the incident acoustic mode, and in Fig. 5(b) with the incident vorticity mode, but with smaller amplitudes. For a value of ε which has been divided by 2, the oscillations of the vorticity mode, due to the presence of the acoustic mode, have also been divided by 2, confirming the asymptotic character of that phenomenon. On the other hand, the amplitudes of the nonadiabatic transitions have diminished on a totally different scale, and they are so small here that they are barely distinguishable, confirming their exponentially small behavior.

In the end, the adiabatic base gives modes which are very close to exact solutions except that they do not take into account two types of phenomena. The first one is the vortical behavior that the acoustic mode is supposed to exhibit, and

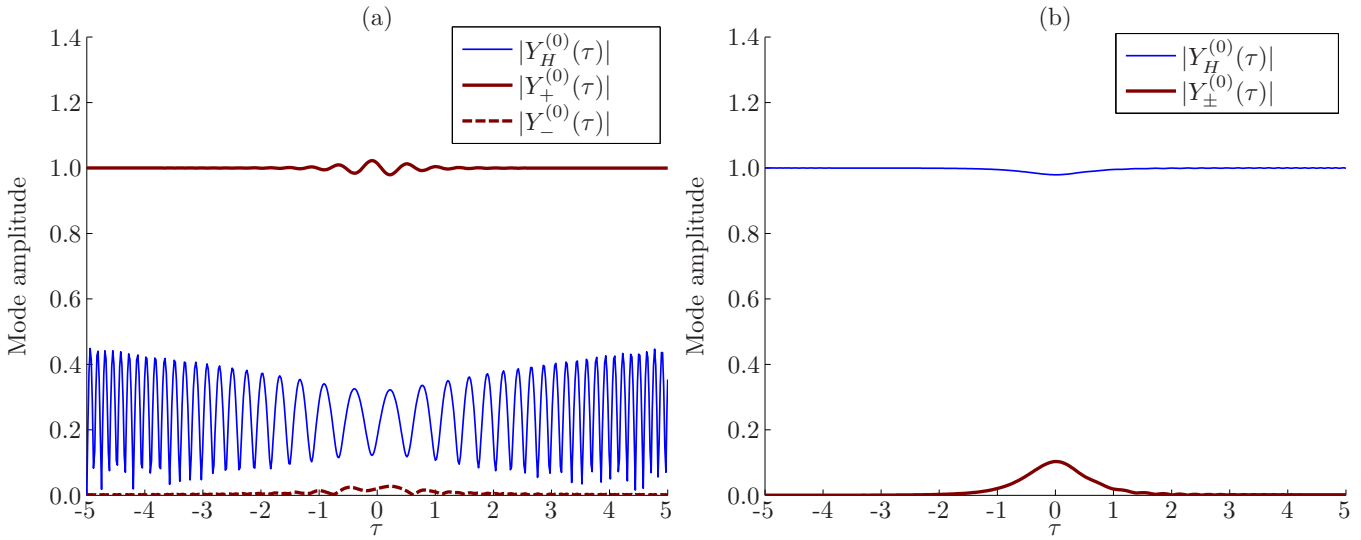

FIG. 5. (Color online) Time evolution of the modulus of the mode amplitudes in the WKB adiabatic base for $\tau_i = -5$ and $\varepsilon = 0.1$. (a) Incident acoustic mode and (b) incident vorticity mode. Same representation as in Fig. 4.

which causes the vorticity modes amplitude to oscillate in the presence of an acoustic mode. The second type of phenomena are the nonadiabatic transitions which permit the generation of a mode by another, but that are exponentially small in $1/\varepsilon$. Two types of transitions are possible: the generation of the two acoustic modes by the vorticity mode, and the generation of an acoustic mode by the other acoustic mode. We wish now to enhance the adiabatic base to smoothen the oscillations during the transitions and to reduce the errors responsible for the oscillations of the vorticity mode amplitude.

IV. THE SUPERADIABATIC BASES

In the following, the WKB modes at order $n \geq 1$ are sought, in the same way as was done by Berry [22,23] in the field of quantum mechanics. Berry showed that the behavior of the amplitudes is dominated by the effect of singularities present in the equations determining the first orders. These singularities are the complex zeros of the eigenvalues. At higher orders, by mean of successive integrations, their effect becomes of significant order even on the real axis. By iterating the order n of the base used to represent the exact solution, the mode amplitudes renormalize and tend to a general form which is the Gauss error function, at a particular order. At the following orders, the asymptotic development starts to diverge.

To apply this result in our case, we look for next-order WKB modes. We need to determine the $\boldsymbol{\varphi}_j^{(n)}$ (with $j \in \{-,H,+\}$) for $n \geq 1$ in the WKB ansatz (16). The starting point is Eq. (18) with the expression (20) of each $\boldsymbol{\varphi}_j^{(n)}$. To perform this calculus, it is convenient to express the $\boldsymbol{\varphi}_j^{(n)}$ vectors in the base of the eigenvectors $\boldsymbol{\varphi}_j^{(0)}$ of H_0:

$$\boldsymbol{\varphi}_j^{(n)} = S\mathbf{c}_j^{(n)} \quad \text{for} \quad j \in \{-,H,+\}, \tag{23}$$

where

$$S = \left[\boldsymbol{\varphi}_-^{(0)}\ \boldsymbol{\varphi}_H^{(0)}\ \boldsymbol{\varphi}_+^{(0)}\right], \tag{24}$$

and where $\mathbf{c}_j^{(n)}$ is the representation of $\boldsymbol{\varphi}_j^{(n)}$ in this base. Note that the matrix S differs from the adiabatic base matrix $\Phi^{(0)}$ because of the exponential terms. Also for convenience, and following the method of Berry, we express the components of H_0 (which are the horizontal and vertical components of the wave vector) in polar coordinates:

$$\begin{bmatrix} 1 \\ \beta(\tau) \end{bmatrix} = k(\tau) \begin{bmatrix} \sin\theta(\tau) \\ \cos\theta(\tau) \end{bmatrix}. \tag{25}$$

Projecting Eq. (18) on this base yields

$$(\lambda_j I - D)\mathbf{c}_j^{(n+1)} = \left(S^{-1}H_1 S - S^{-1}\dot{S} - \frac{d}{d\tau}\right)\mathbf{c}_j^{(n)} \tag{26}$$

for $j \in \{-,H,+\}$, where I is the identity matrix and $D = \mathrm{diag}(\lambda_-,\lambda_H,\lambda_+)$ is the diagonal matrix composed of the eigenvalues λ_j of H_0. A detailed expression of Eq. (26) is given in Eq. (A1) of the Appendix. This allows us to compute all the $\mathbf{c}_j^{(n)}$ through the scheme

$$c_{j,l}^{(n+1)} = \frac{1}{\lambda_j - \lambda_l}\sum_m M_{j,m}c_{j,m}^{(n)} - \dot{c}_{j,l}^{(n)} \quad \text{for} \quad j \neq l, \tag{27a}$$

$$\dot{c}_{j,j}^{(n+1)} = \sum_m M_{j,m}c_{j,m}^{(n+1)} \quad \text{for} \quad j = l, \tag{27b}$$

where $M_{j,m}$ are the coefficients of the matrix $M = S^{-1}H_1 S - S^{-1}\dot{S}$, which has a null diagonal. Of course, expressions of the $\mathbf{c}_j^{(n)}$ at order 0 are $\mathbf{c}_-^{(0)} = (1,0,0)$, $\mathbf{c}_H^{(0)} = (0,1,0)$, and $\mathbf{c}_+^{(0)} = (0,0,1)$. The constants coming from the integration of Eq. (27b) are chosen in order to cancel terms which differ between $\mathbf{c}^{(n)}$ and $\mathbf{c}^{(0)}$ at $\tau = \pm\infty$, so that ideally $\mathbf{c}^{(0)}(\pm\infty) = \mathbf{c}^{(n)}(\pm\infty)$. However, some terms appearing while solving the scheme (27) cannot be canceled because they do not have a finite limit at $\pm\infty$. They are the source of nonuniformities discussed in Ref. [17]. The order $n = 1$ components can be easily

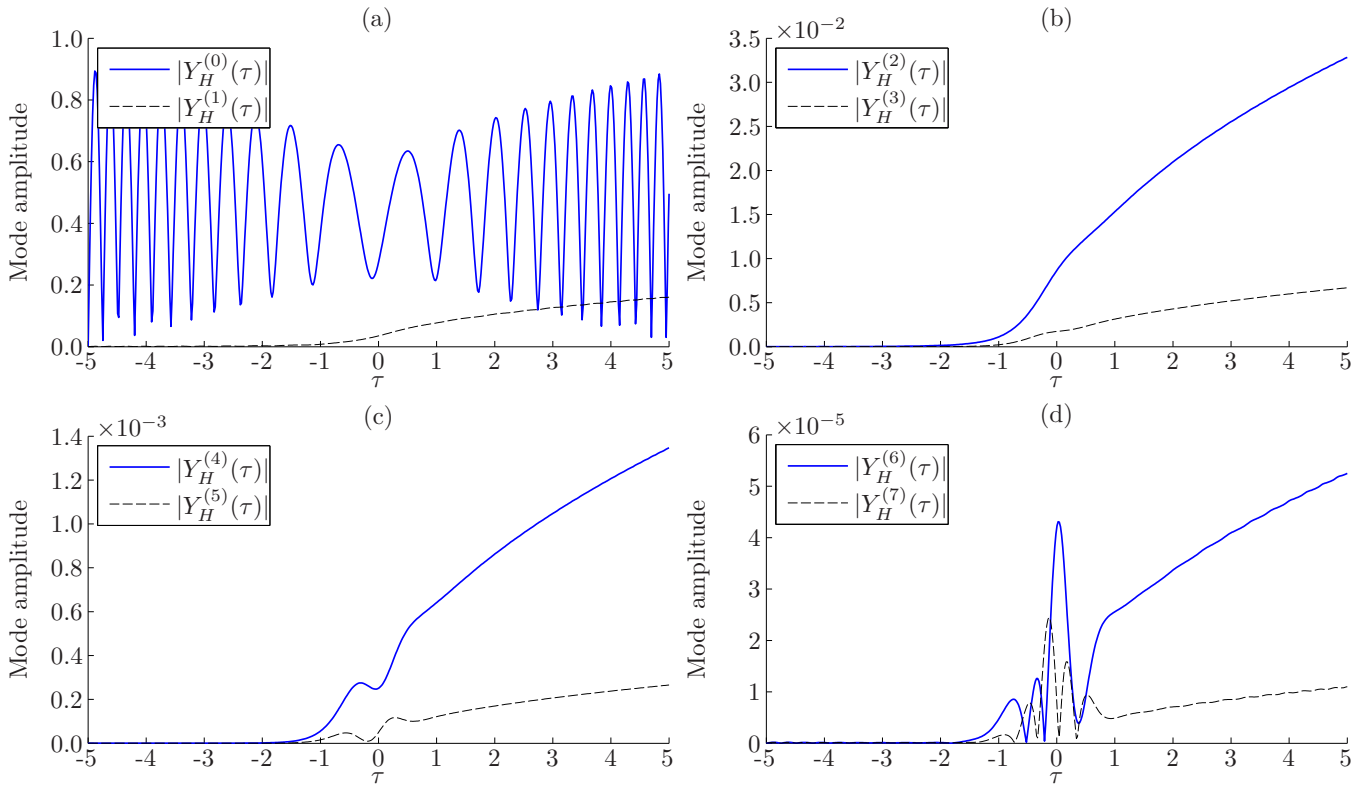

FIG. 6. (Color online) Time evolution of the successive vorticity amplitudes $|Y_H^{(n)}(\tau)|$ on the order n WKB vorticity mode of the superadiabatic base in the case of an incident acoustic "+" mode (of same order), and for $\tau_i = -5$ and $\varepsilon = 0.2$ [cf. Fig. 4(a)]. The mode amplitudes $|Y_H^{(n)}(\tau)|$, $|Y_+^{(n)}(\tau)|$, and $|Y_-^{(n)}(\tau)|$ are computed by projection of the exact solution onto the superadiabatic base of order n, composed of the superadiabatic modes $\mathbf{X}_H^{(n)}(\tau)$, $\mathbf{X}_+^{(n)}(\tau)$, and $\mathbf{X}_-^{(n)}(\tau)$ obtained with the WKB method at order n. The initial condition is imposed on the WKB acoustic "+" mode of same order, that is, $\mathbf{X}(\tau_i) = \mathbf{X}_+^{(n)}(\tau_i)$. Note that the $|Y_H^{(0)}(\tau)|$ curve in (a) is the same as the one in Fig. 4(a).

obtained:

$$\mathbf{c}_-^{(1)} = \begin{bmatrix} -i\cos^3\theta/24 + i\cos\theta - 23i/24 \\ -i\sin^{-1/2}\theta \\ -i\cos\theta\sin^2\theta/4 \end{bmatrix}, \tag{28}$$

$$\mathbf{c}_H^{(1)} = \begin{bmatrix} -i\sin^{9/2}\theta \\ 0 \\ i\sin^{9/2}\theta \end{bmatrix}, \tag{29}$$

$$\mathbf{c}_+^{(1)} = \begin{bmatrix} i\cos\theta\sin^2\theta/4 \\ i\sin^{-1/2}\theta \\ i\cos^3\theta/24 - i\cos\theta + 23i/24 \end{bmatrix}. \tag{30}$$

Because of the successive integrations of Eq. (27), the following terms have an increasing complexity and so are computed with the symbolic computation software MAXIMA [35]. As an example, expressions of the order $n = 2$ coefficients obtained by this method are given in the Appendix.

In the same manner as in the preceding section, we look at the mode amplitudes in the bases formed by these new WKB modes at order n. We define the *superadiabatic base of order n* as the base formed by the order n WKB modes $\{\mathbf{X}_-^{(n)}; \mathbf{X}_H^{(n)}; \mathbf{X}_+^{(n)}\}$, where each $\mathbf{X}_j^{(n)}$ includes now the asymptotic power series from $\boldsymbol{\varphi}_j^{(0)}$ to $\boldsymbol{\varphi}_j^{(n)}$. We define the transformation matrix $\Phi^{(n)} = [\mathbf{X}_-^{(n)}\mathbf{X}_H^{(n)}\mathbf{X}_+^{(n)}]$ and write similarly to Eq. (22)

$$\mathbf{X} = \Phi^{(n)}\mathbf{Y}^{(n)}. \tag{31}$$

To study the effect of the use of the superadiabatic bases, we first focus on the case of the incident acoustic "+" mode. Each figure from Figs. 6(a) to 6(d) represents the time evolution of the order n and order $n+1$ WKB vorticity mode amplitudes from $n = 0$ to 6 in the case of an incident acoustic "+" mode for $\tau_i = -5$ and $\varepsilon = 0.2$ [same configuration as in Fig. 4(a)]. The $|Y_H^{(0)}|$ curve in Fig. 6(a), corresponding to the adiabatic base (order $n = 0$), is of course the same as the corresponding curve in Fig. 4(a), while the $|Y_H^{(1)}(\tau)|$ curve corresponds to the new first superadiabatic base (order $n = 1$). At order $n = 1$, the oscillations disappear and the overall amplitude is diminished by an order. Figures 6(b)–6(d) exhibit a typical asymptotic converging behavior with the amplitudes being diminished by the same factor at each iteration of the order n of the base. The only exception is near the coupling area at $\tau = 0$, where, starting from the order $n = 4$, localized oscillations start to appear, which comes with no surprise since its the area where the nonadiabatic transition takes place. We can see, therefore, that the vortical behavior of the acoustic mode is accurately taken into account in the superadiabatic base for orders $n \geqslant 1$.

Figures 7(a)–7(d) show, under the same conditions, the time evolution of the mode amplitudes of the nonincident acoustic "−" mode, in the same way as Figs. 6(a)–6(d) do for the vorticity mode. As in Fig. 6(a), the $|Y_-^{(0)}(\tau)|$ curve in Fig. 7(a) stands for the adiabatic base and is the same as the corresponding curve in Fig. 4(a). Switching from the

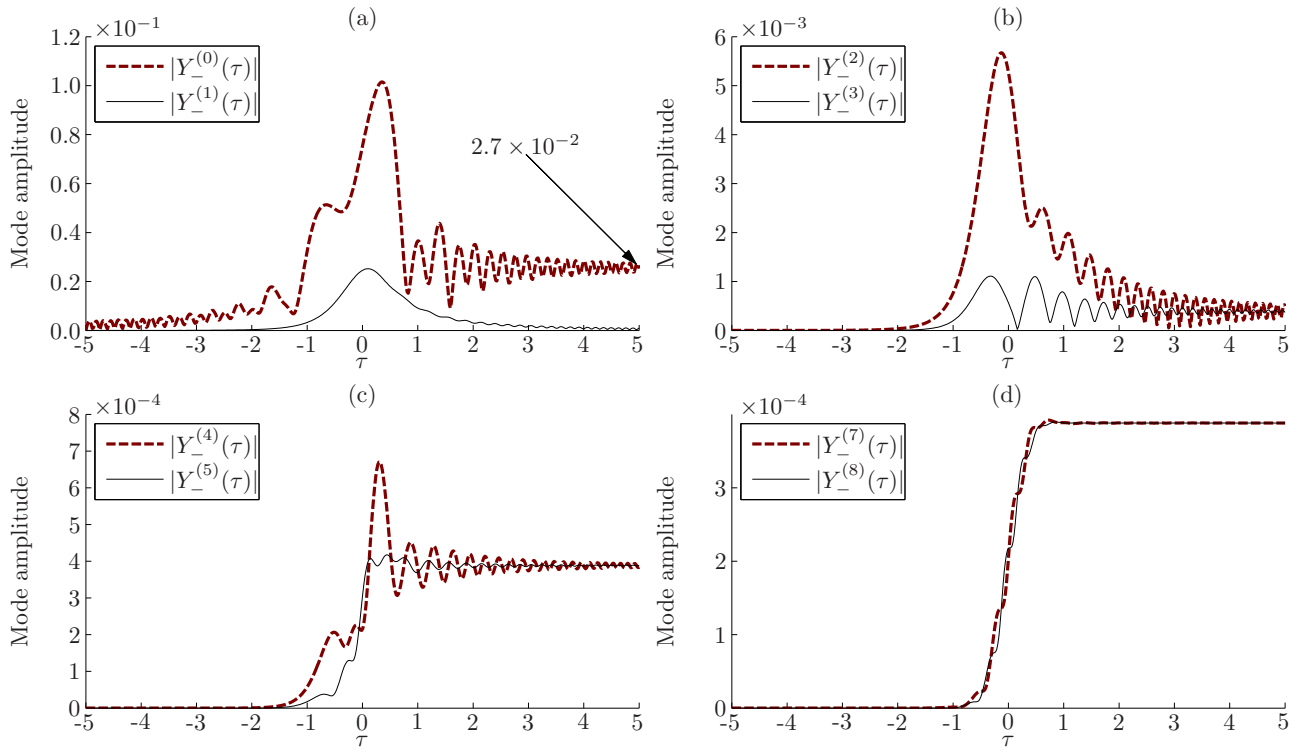

FIG. 7. (Color online) Time evolution of the successive acoustic amplitudes $|Y_-^{(n)}(\tau)|$ on the order n WKB acoustic "$-$" mode of the superadiabatic base in the case of an incident acoustic "+" mode (of same order), and for $\tau_i = -5$ and $\varepsilon = 0.2$ [cf. Fig. 4(a)]. Note that the $|Y_-^{(0)}(\tau)|$ curve in (a) is the same as the one in Fig. 4(a). The optimal order is $n = 8$ in (d).

adiabatic base to the first superadiabatic base has the effect of significantly lowering the oscillations in the coupling area near $\tau = 0$, but also the final amplitude for large time. This latter result could seem surprising with regard to what was said before about the superadiabatic bases being supposed to be unable to take into account nonadiabatic transitions. However, we must remember that the acoustic mode of the adiabatic base contains the error responsible for the strong oscillation of the vorticity mode [Fig. 4(a)]. Injecting the acoustic mode of the adiabatic base as an initial condition leads in fact to injecting a small amount of vorticity mode, which compensates for the error made at order $n = 0$. Therefore, the transition viewed in the adiabatic base is in fact the sum of two transitions: the transition due to the incident acoustic mode and the transition due to that small amount of vorticity mode. On the contrary, the order 1 superadiabatic acoustic mode takes into account that small part of the vorticity that the acoustic mode is supposed to possess. As can be seen in Fig. 6(a), when injecting that order 1 superadiabatic acoustic mode, there is no appearance of the vorticity mode before the coupling area at $\tau = 0$, and the transition we can see on the other acoustic mode is the transition actually due to the acoustic mode. In the end, the difference in the final amplitudes between orders $n = 0$ and 1 is in fact due to a converging process asymptotic to ε^n, and is not due to an exponentially small quantity being taken into account by the superadiabatic base. This can be confirmed by looking at Figs. 7(b)–7(d), which show the renormalization process. At each iteration of the order of the base, the oscillations during the transition near $\tau = 0$ are reduced by one order and get smoothed. But the final amplitude remains the same. Eventually, at the order $n = 8$, displayed in Fig. 7(d), the process of renormalization reaches an optimum and the mode amplitude tends to the Gauss error function, as predicted. However, despite using superadiabatic bases the transition remains present since it is an exponentially small quantity of order $\sim e^{-C/\varepsilon}$, where C is a constant determined by the dynamic near $\tau = 0$. This exponentially small behavior makes it impossible to be described in terms of powers of ε, which is why an asymptotic method such as the WKB method fails to predict it. The determination of the constant C has been performed in the case of the two-dimensional Schrödinger equation (see, for instance, [22]), but is here more difficult, and is beyond the scope of this paper. It would constitute a natural and interesting sequel to this work. Despite not being able to take into account this transition, the superadiabatic base provides a frame that emphasizes the transition.

We now consider the case of an incident vorticity mode. Figures 8(a)–8(d) report the time evolution of the two acoustic mode amplitudes (they are equal) at successive orders in the same way as in Figs. 6 and 7, but for an incident vorticity mode. Here, the curve corresponding to the order $n = 0$ is the same as in Fig. 4(b). Similarly to the preceding case, we can notice the renormalization process which smoothes the oscillations during the transition, and reaches an optimum at $n = 4$ in Fig. 8(c). Then, for orders from $n = 5$ to 7 in Figs. 6(c) and 6(d), the oscillations reappear, grow again, and the process starts to diverge. The final amplitude also remains the same for all orders despite some small variations that can be seen on the two first orders in Figs. 8(a) and 8(b), and which are due to the asymptotic convergence of the superadiabatic base. But

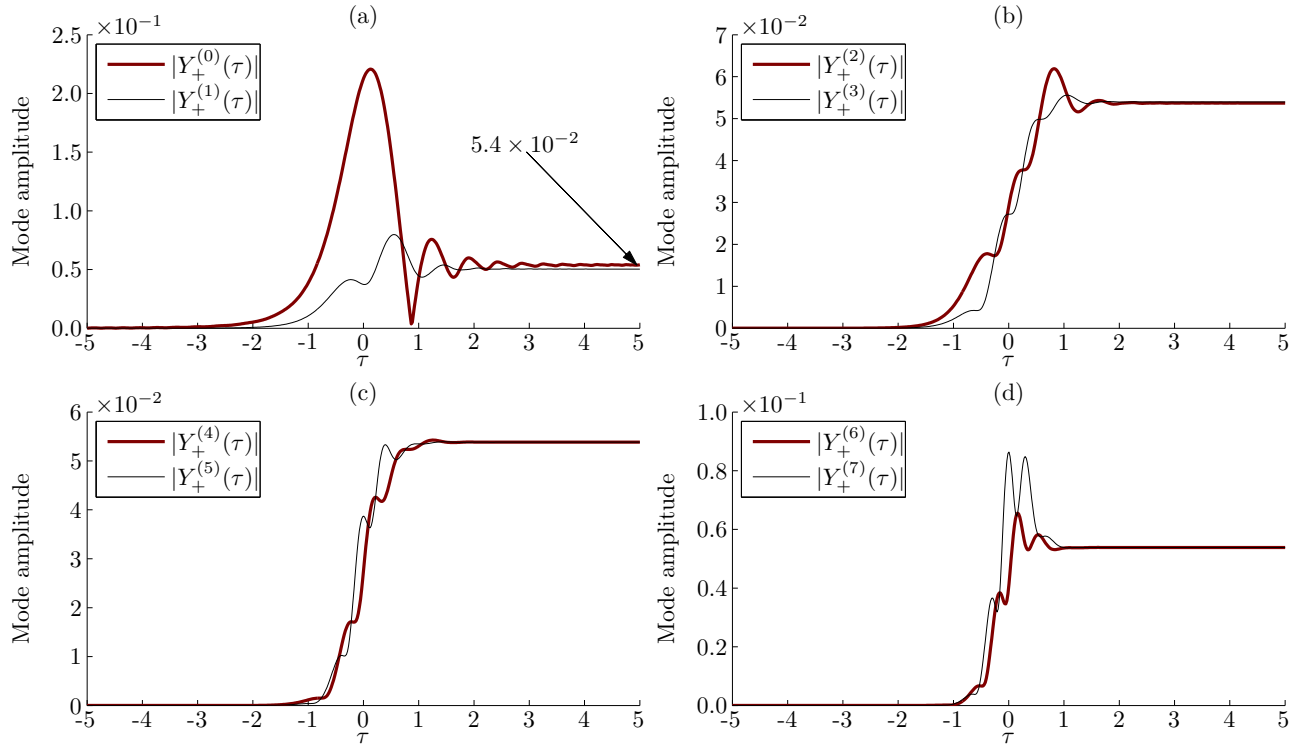

FIG. 8. (Color online) Time evolution of the successive acoustic amplitudes $|Y_+^{(n)}(\tau)|$ on the order n WKB acoustic mode of the superadiabatic base in the case of an incident vorticity mode (of same order), and for $\tau_i = -5$ and $\varepsilon = 0.2$ [cf. Fig. 4(b)]. Note that the $|Y_+^{(0)}(\tau)|$ curve in (a) is the same as the one in Fig. 4(b). The optimal order is $n = 4$ in (c).

the base rapidly converges, and starting from order $n = 3$ the final amplitude does not change.

Figures 9(a) and 9(b) sum up the studied situations by displaying the mode amplitude of all modes represented in their optimal base for the same set of parameters $\tau_i = -5$ and $\varepsilon = 0.2$. Figure 9(a) corresponds to the case of an incident acoustic mode, for which the optimal order is $n = 8$, and Fig. 9(b) corresponds to the case of an incident vorticity mode, for which the optimal order is $n = 4$.

Finally, Fig. 10 shows how the coupling depends on ε. It represents the final amplitude $|Y_+^{(8)}(+\infty)|$ of the acoustic mode as a function of ε (bold line). The curve is indeed asymptotic

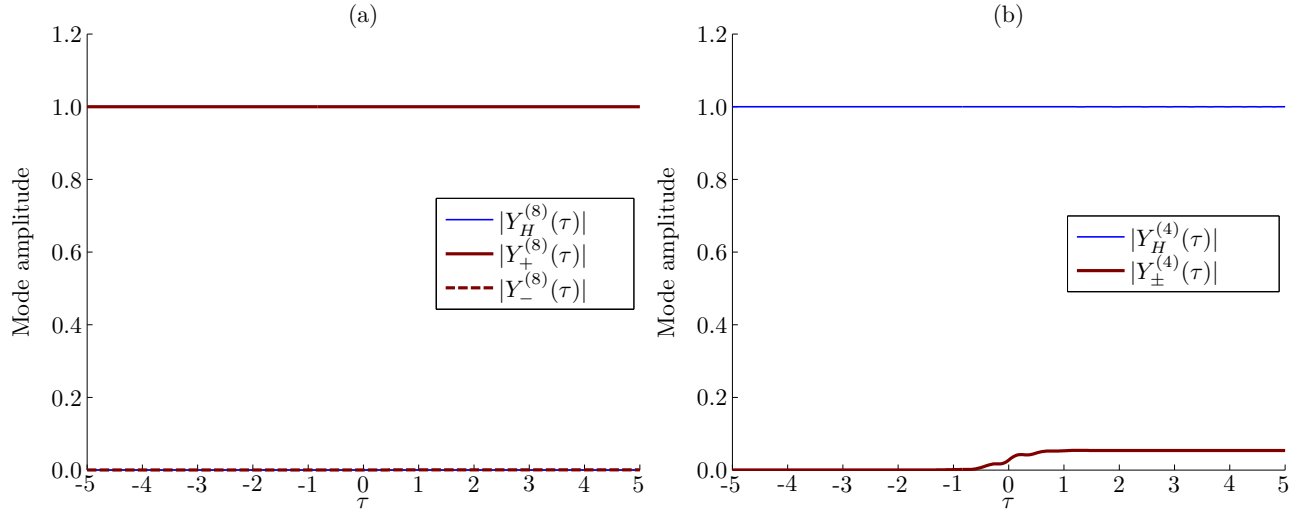

FIG. 9. (Color online) Time evolution of the amplitudes on each WKB mode of the superadiabatic base at optimal order n_{opt}. (a) Incident acoustic mode, optimal order $n_{\text{opt}} = 8$, with initial condition $\mathbf{X}(\tau_i) = \mathbf{X}_+^{(8)}(\tau_i)$. (b) Incident vorticity mode, optimal order $n_{\text{opt}} = 4$, with initial condition $\mathbf{X}(\tau_i) = \mathbf{X}_H^{(4)}(\tau_i)$. The WKB method predicts constant amplitudes, the incident mode amplitude being 1 and the others 0. This figure is to be compared to the mode amplitudes in the simple adiabatic WKB base represented in Fig. 4.

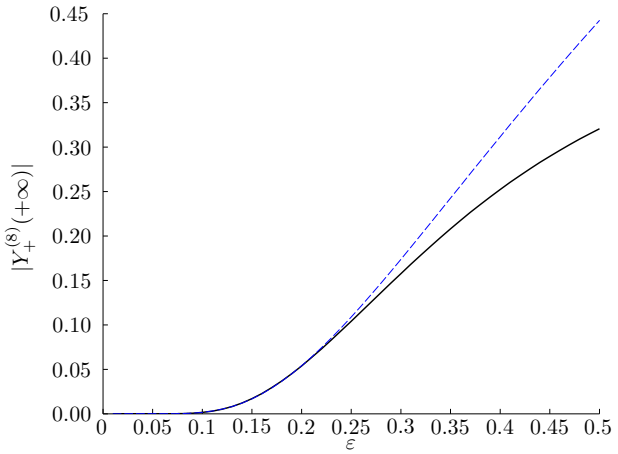

FIG. 10. (Color online) Final amplitude $|Y_+^{(8)}(+\infty)|$ on the acoustic WKB mode of the superadiabatic base at order $n = 8$ as a function of ε for incident vorticity mode (see Fig. 9). Computation (plain line), fitted $\mathcal{A}e^{-\mathcal{C}/\varepsilon}$ curve (dashed line).

to $\mathcal{A}e^{-\mathcal{C}/\varepsilon}$ (thin line). Physically, it represents the amount of acoustic wave created by a vorticity wave as a function of the ratio of the shearing of the steady flow to the frequency of the wave. It is remarkable that for small values of this ratio ($\varepsilon < 0.1$), the coupling is almost nonexistent. It becomes noticeable for values of ε greater than 0.1. From 0 to $\varepsilon = 0.25$ the numerical results fit almost perfectly with the predicted exponential dependence, and then they start to move away from it by growing more slowly. We also recover here results similar to the one obtained by Chagelishvili [1].

To discuss the dependence on the other parameter τ_i, we have to bear in mind that, in the optimal superadiabatic base, the WKB modes describe almost exactly the exact solution. It is only in the coupling area that the WKB modes cannot follow exactly the solution, which is the reason for the nonadiabatic transitions. Therefore, if $\tau_i > 0$, the system will remain described by the incident mode and nothing particular happens in terms of mode coupling since the coupling area at $\tau = 0$ is never crossed. If we take $\tau_i < 0$, as in the cases studied here, but with a different value of τ_i, again the solution remains described by the incident mode before the coupling area at $\tau = 0$, and no difference with the presented results appears. The case in which $\tau_i \sim 0$ is more complicated, and results are a bit erratic in this case. Indeed, one WKB mode is injected at the moment at which the WKB modes fail to cling to the solution, and on the other hand, the nonadiabatic transitions would have already started if the mode was present before. As our work is meant to be a study of a propagating wave arriving in the coupling area, without addressing the question of the generation of that wave, we did not perform a study of that case.

V. CONCLUDING REMARKS

This study focuses on the coupling phenomena existing between acoustic and vorticity perturbations in a Couette plane flow in the context of the WKB method, where the small parameter ε is the ratio of the shear rate of the mean flow to the frequency of the perturbations. This method naturally exhibits three modes of perturbations: two acoustic modes and one vorticity mode. This approach allowed us to recover the two major coupling phenomena which exist between acoustic and vorticity waves in a Couette flow: the generation of acoustic waves by a vorticity wave and the generation of an acoustic wave by another acoustic wave. These two coupling phenomena are closely linked to the time evolution of the wave vector of the wave, as they happen when the wave vector is horizontal and of minimal norm at the same time. They are phenomena of order exponentially small in $1/\varepsilon$, with ε representing the ratio of the shearing of the mean flow to the characteristic frequency of the perturbation. The WKB modes constitute a well-suited base to represent these couplings, since examining the time evolution of the modes in the frame of the superadiabatic bases allows a smooth tracking of the exponentially small emergences of the nonexcited modes. For an optimal order of the superadiabatic base, these emergences take the form the Gauss error function, as can be seen in Fig. 9. This optimal order depends on ε, which is typical of superadiabatic approximations. We believe it gives a simple picture of nonadiabatic couplings between acoustic and vorticity modes. Despite the fact that they inherently present a small vortical behavior which depends on the shearing of the mean flow, the acoustic modes never generate the vorticity mode under this linear frame.

ACKNOWLEDGMENTS

The authors gratefully acknowledge the Agence Nationale de la Recherche (AEROSON project, ANR-09-BLAN-0068-02 program) for financial support.

APPENDIX: DETAILS OF EQ. (26)

In this Appendix, we give the details of Eq. (26). Let us consider a given subscript $_j$ referring to one of the subscripts $_-$, $_H$, or $_+$, so that, for instance, $\boldsymbol{\varphi}_j^{(n)}$ stands for either $\boldsymbol{\varphi}_-^{(n)}$, $\boldsymbol{\varphi}_H^{(n)}$, or $\boldsymbol{\varphi}_+^{(n)}$. Equation (26) is obtained by decomposing the $\boldsymbol{\varphi}_j^{(n)}$ on the base composed of the order 0 components $\boldsymbol{\varphi}_-^{(0)}$, $\boldsymbol{\varphi}_H^{(0)}$, and $\boldsymbol{\varphi}_+^{(0)}$ as stated in Eqs. (23) and (24), and by rewriting in terms of $k(\tau)$ and $\theta(\tau)$ [Eq. (25)] the matrix $S^{-1}H_1S - S^{-1}\dot{S}$ appearing on the right-hand side. This yields

$$\begin{bmatrix} \lambda_j - \lambda_- & 0 & 0 \\ 0 & \lambda_j - \lambda_H & 0 \\ 0 & 0 & \lambda_j - \lambda_+ \end{bmatrix} \begin{bmatrix} c_{j,-}^{(n+1)} \\ c_{j,H}^{(n+1)} \\ c_{j,+}^{(n+1)} \end{bmatrix} = \begin{bmatrix} -\frac{d}{d\tau} & \frac{\sin^2\theta}{k^{3/2}} & -\frac{\cos\theta\sin\theta}{2} \\ -k^{3/2} & -\frac{d}{d\tau} & -k^{3/2} \\ -\frac{\cos\theta\sin\theta}{2} & \frac{\sin^2\theta}{k^{3/2}} & -\frac{d}{d\tau} \end{bmatrix} \begin{bmatrix} c_{j,-}^{(n)} \\ c_{j,H}^{(n)} \\ c_{j,+}^{(n)} \end{bmatrix}. \quad \text{(A1)}$$

Then, all the $\boldsymbol{\varphi}_j^{(n)}$ can be obtained by computing the $c_{j,l}^{(n)}$ coefficients with the scheme given in Eqs. (27). At order 0 the expressions are simply $c_{j,l}^{(0)} = \delta_{j,l}$. We give here the expressions

for orders $n = 1$ and 2.

$$c^{(1)}_{-,-} = -i\frac{\cos^3\theta}{24} + i\cos\theta - \frac{23i}{24}, \tag{A2}$$

$$c^{(1)}_{-,H} = -i\sin^{-1/2}\theta, \tag{A3}$$

$$c^{(1)}_{-,+} = -i\frac{\cos\theta\sin^2\theta}{4}, \tag{A4}$$

$$c^{(1)}_{H,-} = -i\sin^{9/2}\theta, \tag{A5}$$

$$c^{(1)}_{H,H} = 0, \tag{A6}$$

$$c^{(1)}_{H,+} = i\sin^{9/2}\theta, \tag{A7}$$

$$c^{(1)}_{+,-} = i\frac{\cos\theta\sin^2\theta}{4}, \tag{A8}$$

$$c^{(1)}_{+,H} = i\sin^{-1/2}\theta, \tag{A9}$$

$$c^{(1)}_{+,+} = i\frac{\cos^3\theta}{24} - i\cos\theta + \frac{23i}{24}, \tag{A10}$$

$$c^{(2)}_{-,-} = -\frac{\sin^6\theta}{32} + \frac{\sin^4\theta}{32} - \frac{\cos^6\theta}{1152} + \frac{\cos^4\theta}{24} - \frac{23\cos^3\theta}{576} - \frac{\cos^2\theta}{2} + \frac{23\cos\theta}{24} - \frac{529}{1152}, \tag{A11}$$

$$c^{(2)}_{-,H} = \frac{\cos\theta\sin^{\frac{3}{2}}\theta}{4} - \frac{\cos^3\theta}{24\sqrt{\sin\theta}} + \frac{\cos\theta}{\sqrt{\sin\theta}} - \frac{23}{24\sqrt{\sin\theta}}, \tag{A12}$$

$$c^{(2)}_{-,+} = \frac{\sin^6\theta}{8} - \frac{\cos^2\theta\sin^4\theta}{4} + \frac{\sin^4\theta}{2} - \frac{\cos^4\theta\sin^2\theta}{96} + \frac{\cos^2\theta\sin^2\theta}{4} - \frac{23\cos\theta\sin^2\theta}{96}, \tag{A13}$$

$$c^{(2)}_{H,-} = 4\cos\theta\sin^{\frac{13}{2}}\theta, \tag{A14}$$

$$c^{(2)}_{H,H} = -2\sin^4\theta, \tag{A15}$$

$$c^{(2)}_{H,+} = 4\cos\theta\sin^{\frac{13}{2}}\theta, \tag{A16}$$

$$c^{(2)}_{+,-} = \frac{\sin^6\theta}{8} - \frac{\cos^2\theta\sin^4\theta}{4} + \frac{\sin^4\theta}{2} - \frac{\cos^4\theta\sin^2\theta}{96} + \frac{\cos^2\theta\sin^2\theta}{4} - \frac{23\cos\theta\sin^2\theta}{96}, \tag{A17}$$

$$c^{(2)}_{+,H} = \frac{\cos\theta\sin^{\frac{3}{2}}\theta}{4} - \frac{\cos^3\theta}{24\sqrt{\sin\theta}} + \frac{\cos\theta}{\sqrt{\sin\theta}} - \frac{23}{24\sqrt{\sin\theta}}, \tag{A18}$$

$$c^{(2)}_{+,+} = -\frac{\sin^6\theta}{32} + \frac{\sin^4\theta}{32} - \frac{\cos^6\theta}{1152} + \frac{\cos^4\theta}{24} - \frac{23\cos^3\theta}{576} - \frac{\cos^2\theta}{2} + \frac{23\cos\theta}{24} - \frac{529}{1152}. \tag{A19}$$

[1] Y. Auregan, A. Maurel, V. Pagneux, and J. Pinton, *Sound-Flow Interactions* (Springer-Verlag, Berlin, 2002).
[2] K. M. Butler and B. F. Farrell, Phys. Fluids A **4**, 1637 (1992).
[3] S. C. Reddy, P. J. Schmid, and D. S. Henningson, SIAM J. Appl. Math. **53**, 15 (1993).
[4] L. N. Trefethen, A. E. Trefethen, S. C. Reddy, and T. A. Driscoll, Science **261**, 578 (1993).
[5] W. Thomson, Philos. Mag. **24**, 188 (1887).
[6] G. D. Chagelishvili, T. S. Hristov, R. G. Chanishvili, and J. G. Lominadze, Phys. Rev. E **47**, 366 (1993).
[7] G. D. Chagelishvili, A. D. Rogava, and I. N. Segal, Phys. Rev. E **50**, R4283 (1994).
[8] G. D. Chagelishvili, A. D. Rogava, and D. G. Tsiklauri, Phys. Rev. E **53**, 6028 (1996).
[9] G. D. Chagelishvili, G. R. Khujadze, J. G. Lominadze, and A. Rogava, Phys. Fluids **9**, 1955 (1997).
[10] G. D. Chagelishvili, A. G. Tevzadze, G. Bodo, and S. S. Moiseev, Phys. Rev. Lett. **79**, 3178 (1997).
[11] A. D. Rogava and S. M. Mahajan, Phys. Rev. E **55**, 1185 (1997).
[12] S. M. Mahajan and A. D. Rogava, Astrophys. J. **518**, 814 (1999).
[13] A. Rogava, S. Poedts, and S. Mahajan, J. Comput. Acoust. **9**, 869 (2001).
[14] G. Gogoberidze, G. D. Chagelishvili, R. Z. Sagdeev, and D. G. Lominadze, Phys. Plasmas **11**, 4672 (2004).
[15] J. George and R. I. Sujith, Phys. Rev. E **80**, 046321 (2009).
[16] W. Mohring, E. Muller, and F. Obermeier, Rev. Mod. Phys. **55**, 707 (1983).
[17] G. Favraud and V. Pagneux, Proc. R. Soc. London, Ser. A **469**, 20120708 (2013).
[18] J. P. Boyd, Acta Appl. Math. **56**, 1 (1999).
[19] L. D. Landau, Phys. Z. Sowjetunion **2**, 46 (1932).
[20] L. Landau and E. Lifshitz, *Course of Theoretical Physics*, Vol. 3 (Butterworth-Heinemann, Oxford, 1977).
[21] C. Zener, Proc. R. Soc. London, Ser. A **137**, 696 (1932).
[22] M. V. Berry, Proc. R. Soc. London, Ser. A **429**, 61 (1990).
[23] R. Lim and M. V. Berry, J. Phys. A **24**, 3255 (1991).
[24] A. M. Dykhne, Sov. Phys. JETP **14**, 941 (1962).
[25] J. P. Davis and P. Pechukas, J. Chem. Phys. **64**, 3129 (1976).
[26] G. A. Hagedorn and A. Joye, Commun. Math. Phys. **250**, 393 (2004).
[27] V. Betz, B. D. Goddard, and S. Teufel, Proc. R. Soc. London, Ser. A **465**, 3553 (2009).
[28] R. Lim, J. Phys. A **26**, 7615 (1993).
[29] M. Elk, Phys. Rev. A **52**, 4017 (1995).
[30] E. J. Hinch, *Perturbation Methods* (Cambridge University Press, Cambridge, 1991).
[31] J. Schiff and S. Shinider, SIAM J. Numer. Anal. **36**, 1392 (1999).
[32] A. Iserles, A. Marthinsen, and S. P. Nørsett, BIT **39**, 281 (1999).
[33] A. Iserles and S. P. Norsett, Philos. Trans. R. Soc. A **357**, 983 (1999).
[34] V. Pagneux, J. Comput. Appl. Math. **234**, 1834 (2010).
[35] Maxima, A Computer Algebra System (Version 5.30.0), 2013, http://sourceforge.net/projects/maxima/